iScience, Volume *23*

Supplemental Information

Synergizing Photo-Thermal H_2 and Photovoltaics into a Concentrated Sunlight Use

Sanli Tang, Xueli Xing, Wei Yu, Jie Sun, Yimin Xuan, Lu Wang, Yangfan Xu, Hui Hong, and Hongguang Jin

Supplemental Information

Supplemental Data Items

Morphology stability and selective absorption of Au-TiO_2

To test the distribution of Au on TiO_2 nanoparticles, we examined the morphology of the nanocatalyst using scanning electron microscopy (SEM) and transmission electron microscopy (TEM). **Figure S1** shows that the catalyst is composed of TiO_2 nanoparticles of ~ 50 nm, while the Au NPs are uniformly deposited on the surface of the TiO_2 nanoparticles. High-resolution TEM in **Figure S1** shows that the average diameter of Au NPs is 10-15 nm.

The stability of the nanostructures under high-intensity sunlight was also examined. **Figures S1** and **S2** compare the TEM and SEM images before and after 40 h experiments under the sunlight intensity of 15 kW m^{-2}. The morphology of Au-TiO_2 remained stable. Neither the deposition nor the morphology of the Au nanocrystals changed after the experiments. The HRTEM image also demonstrates that the Au NPs remain an average diameter of 10–15 nm and show no sign of agglomeration after the experiment.

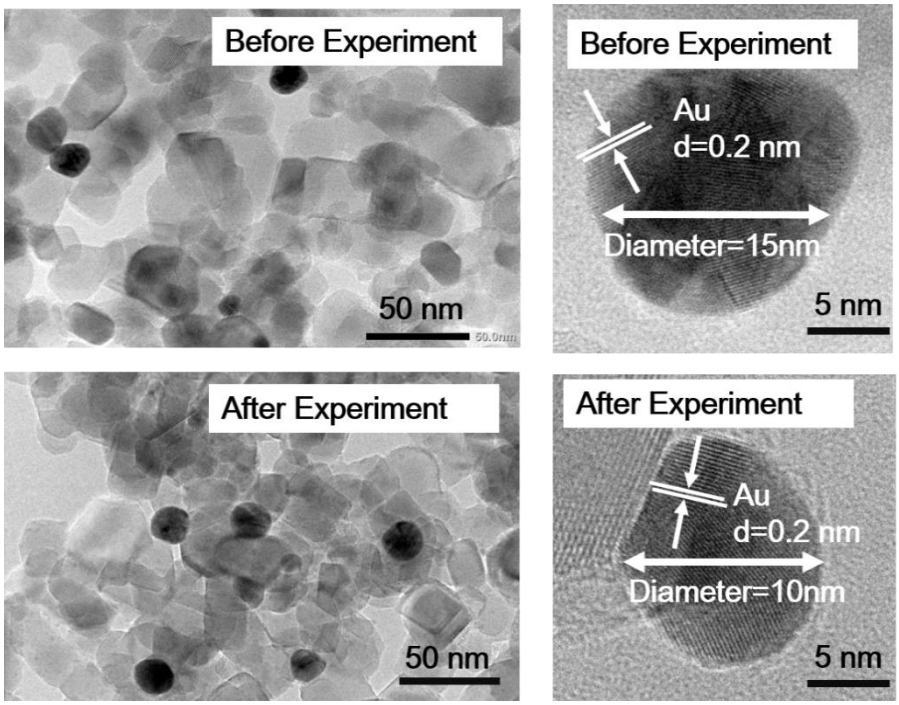

Figure S1. TEM and HRTEM image of the Au-TiO_2 photo-thermal catalyst, related to **Figure 2**.

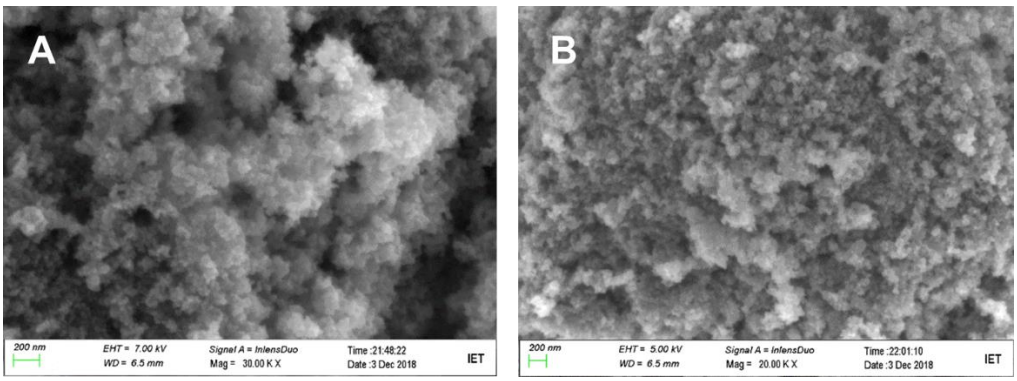

Figure S2. SEM image (A) before and (B) after 40 hours of hydrogen evolution experiments, related to **Figure 2**.

Before integrating PV into the system, we measured the transmitted sunlight intensity and spectrum distribution. The measurements were done on an Agilent Cary5000 UV-Vis-IR spectrometer. **Figure S3** shows that the unabsorbed sunlight is at the 600–1200 nm band and is close to that of a band-pass optical beam splitter (Vincenzi et al., 2010), which matches the mono-Si PV bandgap. To further adapt to various PV materials, we can conveniently shift the transmitted spectrum by controlling the size and shape of Au-TiO_2 and changing the optical thickness and mass concentration of the reaction solution. In this study, the mass concentration of 0.1–1.0 g L^{-1} can control the transmittivity at 600–1200 nm at 10–70%.

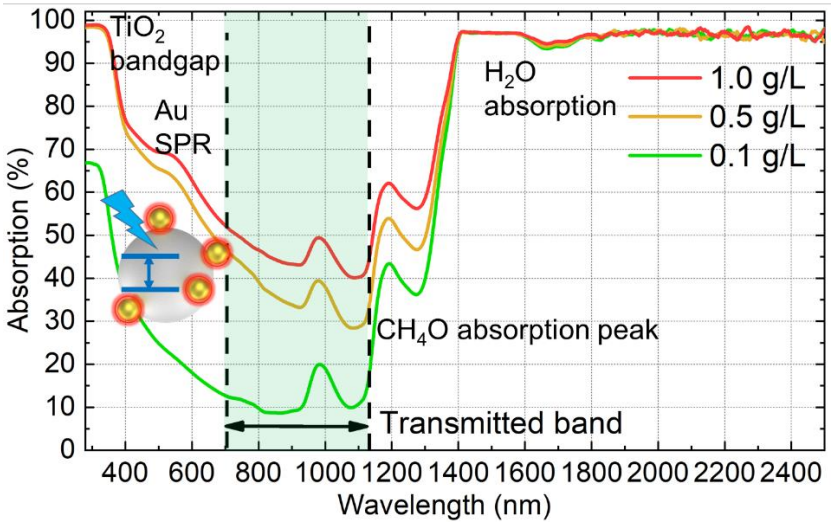

Figure S3. Absorption spectra of the reaction solution at catalyst concentration of 0.1–1.0 g L^{-1} in 10 vol. % methanol aqueous solution, related to **Figure 2** and **7**.

Simulated electromagnetic absorption of Au-TiO_2

The increase in the H_2 production rate benefits from the Au loading, which broadens the transport channel for charge carriers. We used the FEM method to simulate the effect of plasmonic Au (diameter 15 nm) on the light absorption of TiO_2 (diameter 30 nm) nanoparticles (**Figure S4A**). **Figure S4A** shows that at 400 nm wavelength, TiO_2 nanoparticles have a bulk phase absorption of ~10^2 times higher than the surface owing to the semiconductor excitation and corresponding absorption. For the wavelength at 400–600 nm, the absorption is pronounced on the surface, ~2×10^3 times the bulk of Au NPs because of the surface plasmon enhancement. Such enhancement also activates the TiO_2 surface, which has a 10^3 enhancement in the electrical field than the bulk part of TiO_2 in **Figure S4B**. **Figures S4A** and **S4B** reveal that the SPR effect of Au NPs can result in an intensified localized electric field, enhancing the charge carrier generation and separation on the surface. **Figure S4C** shows that the Au NPs at diameters of 10 and 15 nm have a stronger surface plasmon resonance (SPR) effect in the ultraviolet-visible narrow band than Pt NPs, enhancing the selectivity for transmitted sunlight.

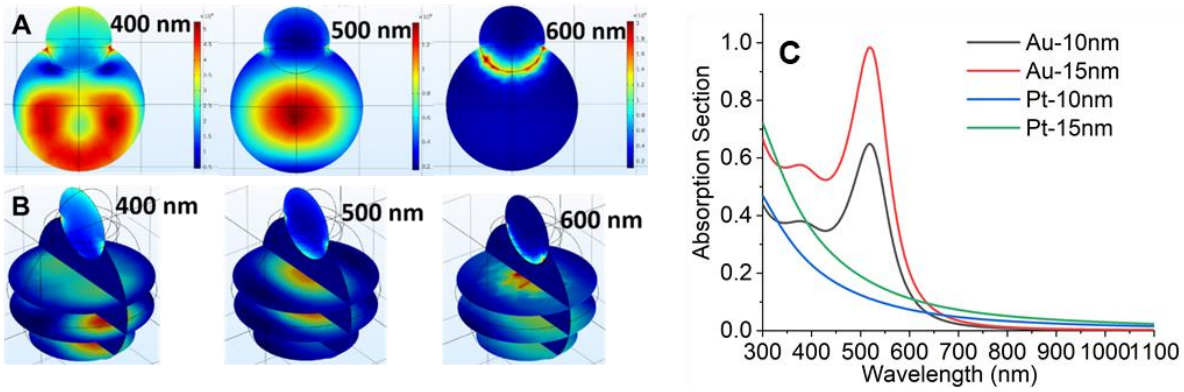

Figure S4. Electromagnetic simulation of Au-TiO_2 immersed in 10 vol % methanol aqueous solution, related to **Figure 3**. (A) The norm of the total electrical field vector and (B) the absorption of incident light under 400–600 nm irradiation. (C) The comparison of loaded metallic particles in absorption spectra.

Details for comparison with benchmark photo-thermal or thermal catalysis

Table S1 shows the details of the benchmark research in photo-thermal catalytic H_2 generation from methanol aqueous solution (see **Figure 3**). Note that some research used a strong light intensity in UV band. For convenience in comparison, the equivalent solar concentration ratio of such research was calculated by dividing the employed UV light intensity by its proportion in full-spectrum energy. In other words, the equivalent solar concentration ratio means how many suns are needed to provide the input UV light used in the reported experiment.

Table S1. Experimental details of the references, related to **Figure 3.**

Material	Intensity (kW m^{-2}) @Wavelength band	Equivalent intensity (suns)	Reaction temperature(°C)	H_2 generation rate (mL g_{cat}^{-1} h^{-1})	Reference in **Figure 3**
SiO_2/Ag@TiO_2	0.353 @365 nm, plus 1 @>400 nm	7.5	90	173.6	12
Pt/TiO_2	6.5 @AM1.5	6.5	55	268.8	18
Pt/TiO_2	6 @AM1.5	6	55	460.3	30
Pt/TiO_2	0.37 @350-450 nm	4.62	55	286.0	6
Pt/TiO_2	0.117@350-400nm	4.62	-	492.8	7
Pt/TiO_2	0.15 @UV band	2.77	65	26.1	15
Pt/TiO_2	2 @>420 nm	2	-	20.7	9

Table S2 shows the details of the benchmark research in thermocatalytic H_2 generation from methanol/water mixture (see **Figure 6**). For convenience in comparison, the equivalent solar concentration ratio of a certain reaction temperature was approximately calculated considering a parabolic trough solar collector.

Table S2. Experimental details of the references, related to **Figure 6.**

Material	Reaction temperature(°C)	Approximate intensity (suns)	H_2 generation rate (mL g_{cat}^{-1} h^{-1})	Reference in **Figure 6**
NiO_x/TiO_2	260	54	1202.9	10
$CuO/ZnO/Al_2O_3$	200	45	99.8	38
$CuO/ZnO/Sc_2O_3$	220	49	1452.0	23
Pt/TiO_2	200	45	34.72	4
Ru/TiO_2	300	60	336.0	5
Cu-Zn-Ti oxide	200	45	1133.4	42
$CuO-CeO_2$	300	60	1062.0	35

The effects of solar SPR loading and solar heating

We studied the interaction between the solar concentration and the SPR effect (**Figure S5A**). Pure P25 TiO_2 was selected for the comparison experiment, in which the H_2 production was <5 mL h^{-1} at *C* = 15. With Au SPR loading, the H_2 generation rate increased over 25 times to 110 mL h^{-1}.

In **Figure S5B**, we experimentally compared the H_2 generation with IR band heating (35–65 °C at *C* = 5–9) to that cooled at room temperature (20 °C at *C* = 5–9). At above 65 °C, the H_2 production with IR band heating becomes 2–3 times that with cooling. Through photo-thermal synergy in this work, the energy grade of the IR band is improved to that of solar H_2. The relationship between solar concentration ratio and steady temperature is: *C* = 3 at 35°C, *C* = 5 at 45°C, *C* = 7 at 55°C, *C* = 9 at 65°C, *C* = 12 at 75°C and *C* = 15 at 82°C.

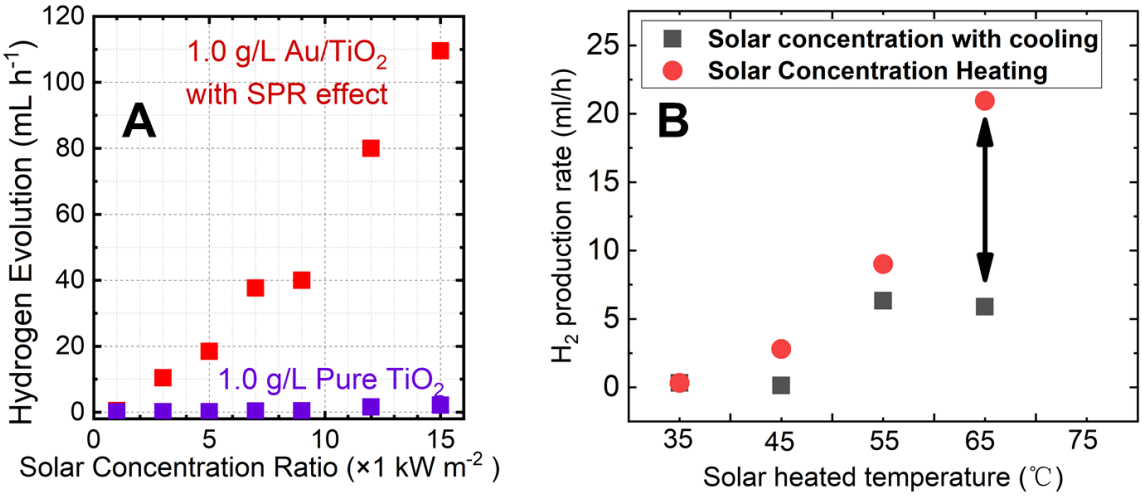

Figure S5. The effects of solar SPR loading and solar heating, related to **Figure 3**. (A) Elevation of H_2 production from SPR Au and photo-thermal effect. (B) The effect of IR band solar heating on H_2 production.

Transient photocurrent

Figure S6 shows the transient photocurrent curve. The transient photocurrent was measured for 1, 5 and 9 suns with light chopping to control the on/off state of incident sunlight. The continuously rising shape of the transient photocurrent was observed for 1, 5 and 9 suns.

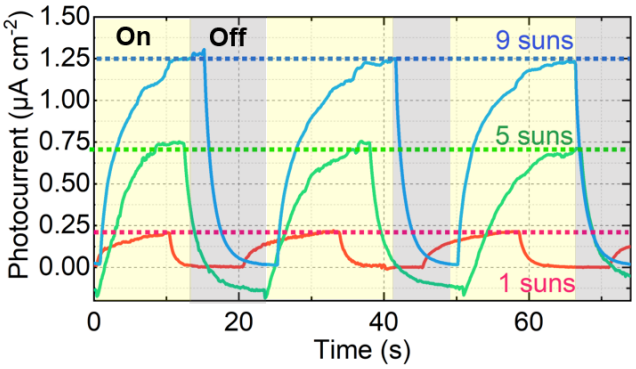

Figure S6. The transient photocurrent curve measured for 1, 5 and 9 suns when the concentrated sunlight is on/off, related to **Figure 4**.

Transmitted solar spectrum energy

In semiconductor-based photocatalysis or photo-thermal catalysis, the unabsorbed and scattered sunlight is transmitted and wasted. In **Figure S7A**, by measuring the transmitted sunlight intensity, for light spot diameter of 3.8 cm, the total input sunlight into the system is 7–21 W. The transmitted sunlight takes a constant proportion in the total sunlight input, which is 20%, 10%, and 5% for 0.1, 0.5, and 1.0 g L^{-1}, respectively. We used a spectrometer to show that the transmitted spectrum consisted of the re-radiated (500 nm), scattered (600 nm), and unabsorbed (700–1100 nm) sunlight by the catalyst (**Figure S7B**). Since the transmitted solar energy takes a considerable percentage and mainly exists in the Vis-NIR band, we chose the mono-silicon PV cell to generate electricity. The bandgap of mono-silicon (1.2–1.3 eV) has a good match with the energy grade of the Vis-NIR band, minimizing the heat relaxation irreversibility.

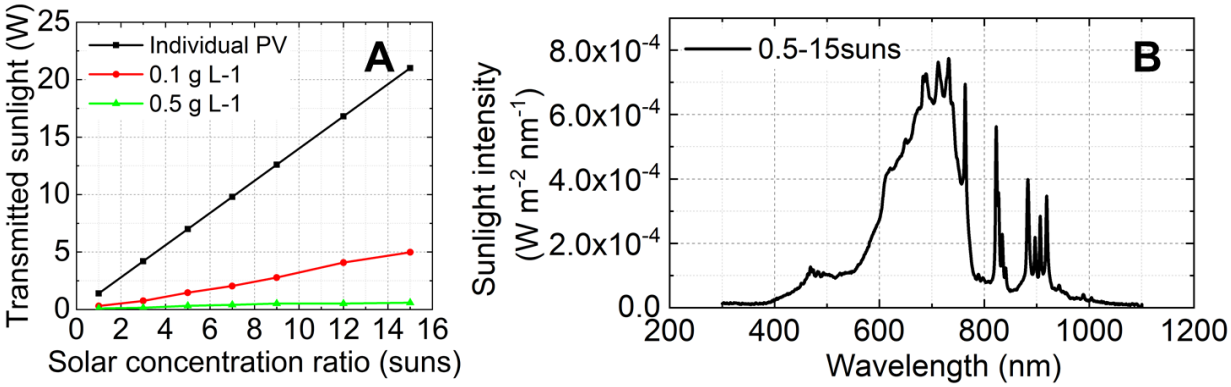

Figure S7. (A) The transmitted sunlight energy from reaction solution of 0.1–1.0 g L^{-1} catalyst concentration. (B) The transmitted spectrum measured at 1.0 g L^{-1} and 15 suns, related to **Figure 7**.

Voltage-current results of the PV cell

Figure S8A–E shows the U-I curve of the PV cell at different catalyst concentrations and sunlight intensity. Moreover, a comparison was also made with an individual PV cell under full-spectrum sunlight.

In **Figure S8F**, the individual PV cell shows a rapid decrease in the current value when the external circuit voltage increases. Such a rapid decrease can result in a lower solar-to-electricity conversion efficiency than the

integrated PV. This indicates that the transmitted spectrum may be most desirable for the mono-silicon PV bandgap.

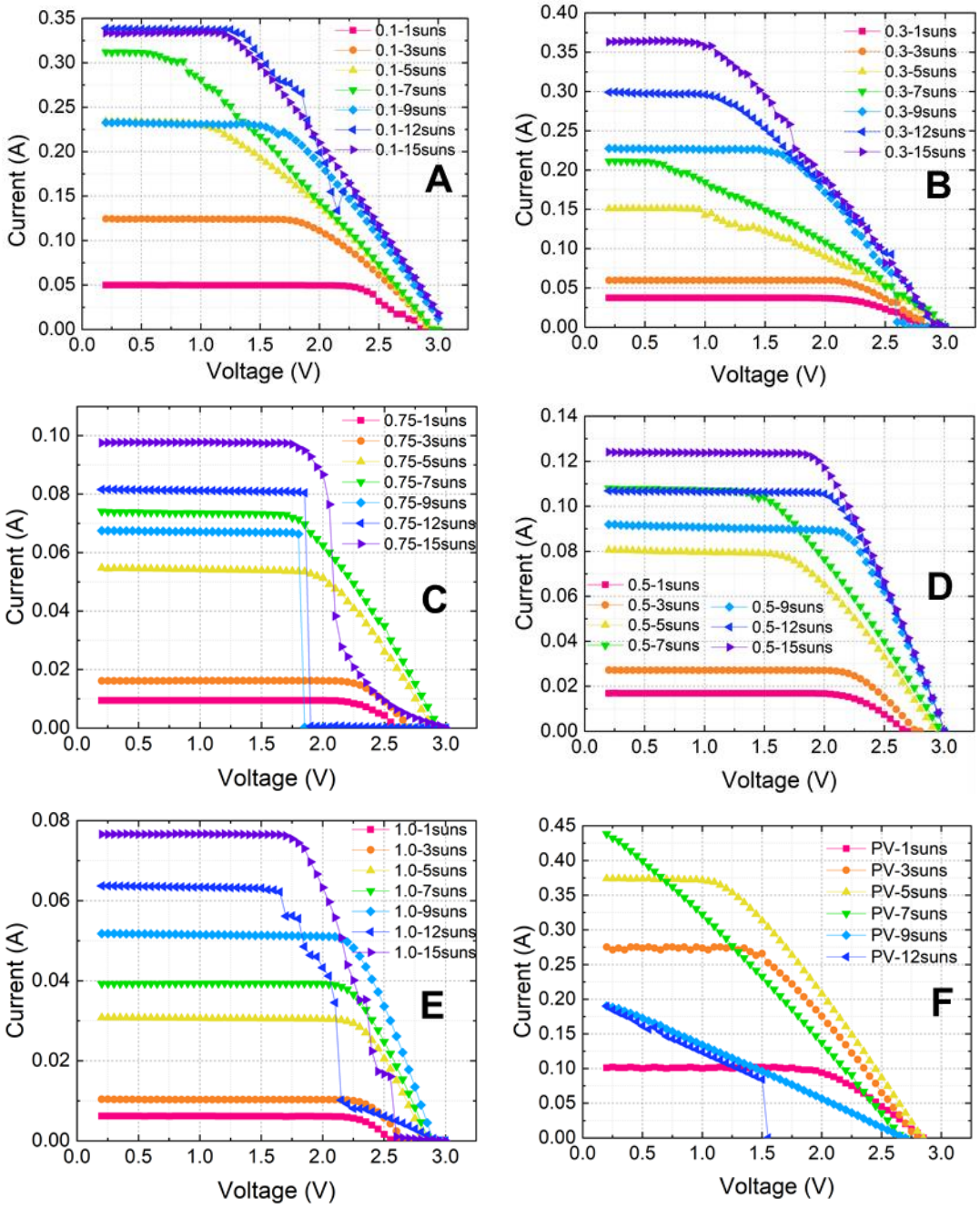

Figure S8. Voltage-current character of the mono-silicon PV cell integrated with (A) reaction system with 0.1 g L^{-1} catalyst (B) reaction system with 0.3 g L^{-1} catalyst (C) reaction system with 0.5 g L^{-1} (D) catalyst reaction system with 0.75 g L^{-1} and (E) catalyst reaction system with 0.3 g L^{-1} catalyst. (F) The voltage current character of an individual PV cell. Related to **Figure 7**.

Energy flow of the individual photo-thermal H_2 and PV generation

We analyzed the energy flow for the individual cases of photovoltaics or 0.5 g L^{-1} photo-thermocatalysis under *C* = 12 (**Figure S9A-B** and **Table S3**). **Figure S9A** shows the energy flow of the individual case of photo-

thermocatalysis. To start with, the input sunlight was concentrated and had an optical loss of 9.75%. In the sunlight absorption process, the photo-thermochemical reaction has a scattering loss of 24.73% and a transmission loss of 17.90%. For the sunlight absorbed by the photo-thermal reaction, the photo effect generates charge carriers (from the UV-Vis band), while the thermal effect generates phonons (from the IR band). Using the extra energy from the UV band, the phonons from the IR band are elevated to solar syngas. The IR phonons not only join the indirect excitation for charge carriers, but also directly activate the adsorbed molecules. In **Figure S9A**, the thermal phonon is depicted to join the UV-Vis band for H_2 production. The photo and thermal effects contribute nearly equally to the H_2 generation process, resulting in H_2 output accounting for 1.21% of the total input sunlight.

Figure S9B shows the energy flow of the individual case of the PV cell. The mono-silicon PV cell has a bandgap suitable for the Vis-NIR band sunlight and may have heat relaxation loss under the full-spectrum input. Moreover, the commercial PV cell is designed for C = 1 and may have a recombination loss at C > 1. Under the concentrated sunlight of C = 12, the combined effect of heat relaxation and recombination in the PV cell leads to an energy loss of 98.10%, with electricity generation accounting for 1.90% of the input sunlight.

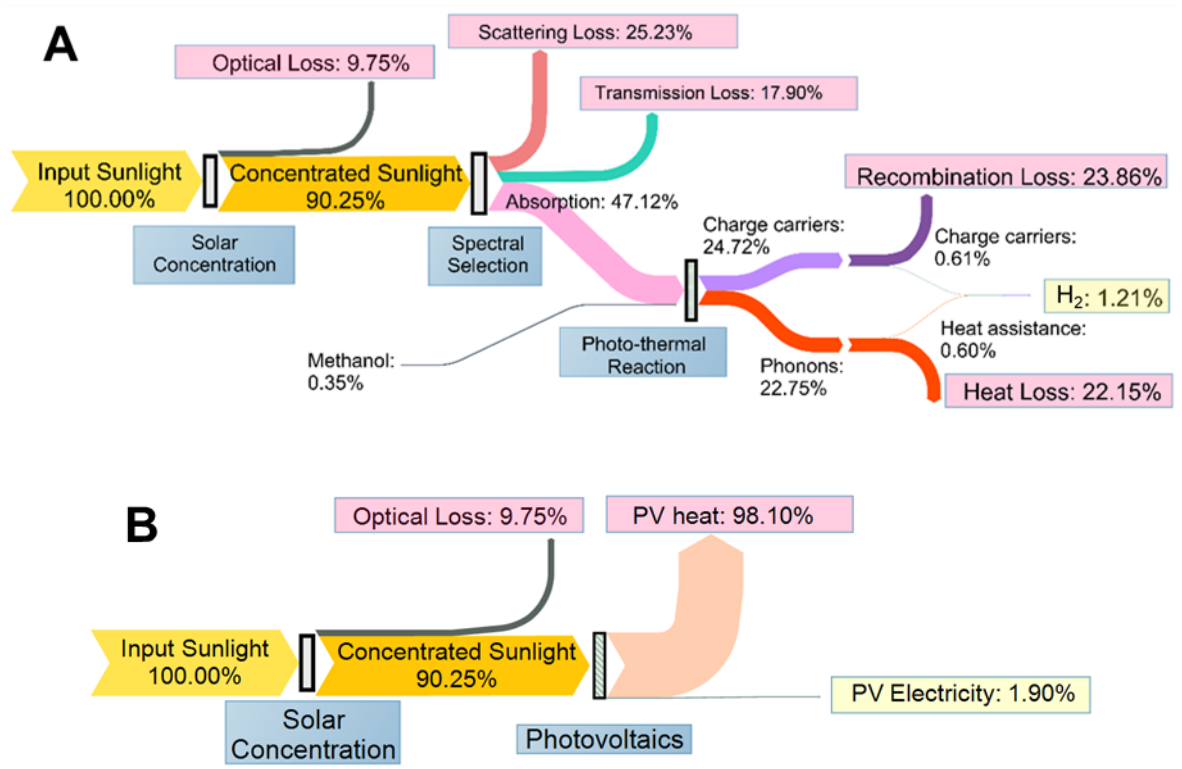

Figure S9. The energy flow chart related to **Figure 9.** (A) Individual case of photo-thermocatalysis and (B) the individual case of PV.

Table S3. Energy loss analysis, related to **Figure 9.**

Terms	Co-production system	Individual photo-thermocatalysis	Individual PV
Input sunlight, *CI*	100%	100%	100%
Input methanol, $\Delta G_{CH_3OH} \cdot n_{CH_3OH}$	0.35%	0.35%	-
Optical loss	9.75%	9.75%	9.75%
Scattering loss, L_{sca}	19.85%	25.23 %	-
Recovered from scattering, R_{sca}	4.88%	-	-
Transmitted sunlight	17.90%	17.90%	90.25%
PV heat, L_{PV}	20.21%	-	88.35%
PV electricity, *P*	2.57%	-	1.9%
Absorbed for H_2 production, $A(\lambda) \cdot CI$	47.62%	47.12%	-
Charge carriers	24.67%	24.37%	-
Phonons/heat	22.95%	22.75%	-
Recombination loss, L_r	23.81%	23.51%	-
Heat loss, L_{heat}	22.10%	22.15%	-
Hydrogen, $\Delta G_{H_2} \cdot n_{H_2}$	1.71%	1.21%	-
Overall conversion efficiency, η_{sys}	4.2%	1.21%	1.9%

Transparent Methods

The experimental apparatus and procedure

Figure S10 shows the experimental apparatus. In **Figure S10A,** the convex lens assembled on the 300 W Xenon lamp (CEL-HXF300, CEAULIGHT) to provide concentrated sunlight. Through controlling the working current and changing the lens and the distance from the reactor to the lamp, the solar concentration ratio is changed at 1–15 suns at the working focus, where the surface of the reaction solution is located. The working focus had a diameter of 60-82 mm for 1-7 suns and a diameter of 40-55 mm for 9-15 suns. **Figure S10B** shows the 82 mm focus for 1 sun and the 55 mm focus for 9 suns. To make comparison on a basis of the same irradiated area but different concentration ratio, the hydrogen generation rate for using a smaller light focus with diameter d_1 was divided by $(d_1/d_2)^2$ before compared with that using a larger focus of diameter d_2. The photos in **Figure S10C** were taken with a filter in front of the camera to avoid overexposure of the picture.

In **Figure S10C**, two types of reactor with inner diameter of d_1 = 82 mm and d_2 = 55 mm is used, to meet the different area of the sunlight focus at different concentration ratios. The reactors were quartz to ensure high sunlight transmittance. Moreover, the side surface of the reactor is coated with a mirrored surface (95% reflectivity) to recover the scattered sunlight. To ensure a same optical thickness of the incident sunlight in the nanofluid, the volume of reaction solution is respectively 100 mL and 50 mL for the two reactors.

Figure S10D shows two square-shaped PV cells fixing on two round-shaped supports. The PV cells are commercially fabricated by connecting in series five Si PV cells with 0.6 V open circuit voltage, thus the rated open circuit voltage is 3.0 V for both PV cells. The areas of the PV cells are respectively 24.5 cm^2 and 15.1 cm^2.

The larger PV cell is integrated with the d_1 = 82 mm reactor, while the smaller one is integrated with the d_2 = 55 mm reactor. Then, both PV cells are connected to a set of aluminum alloy cooling fins to remain near the room temperature during the operation.

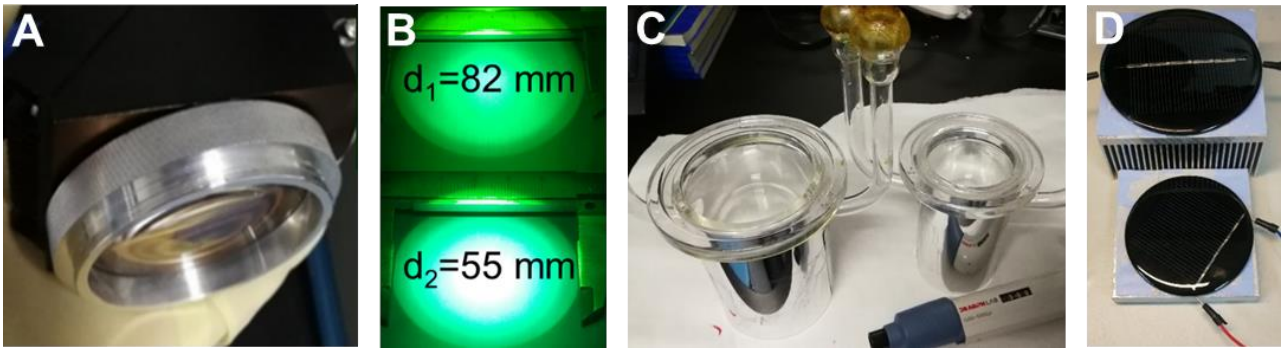

Figure S10. The experimental apparatus related to **Figure 2**. (A) The convex lens on the Xenon lamp. (B) The working focus. (C) The two type of quartz reactors. (D) The photovoltaic cell.

In a typical experiment procedure, the average sunlight intensity on the working focus was measured. As shown in **Figure S11A**, the average sunlight intensity is measured by a five-point average method. The point in the center contributes to 2/3 of the average sunlight intensity, while the average intensity of the other four point on the margin contributes to 1/3 of the average sunlight intensity. The five points are located using a steel plate with a matrix of holes (inset of **Figure S11A**). The sunlight intensity at each point is measured by a light power meter (CEALL- NP2000, CEAULIGHT) with measuring range of 0-20 kW m^{-2}.

After sunlight intensity measurement, a certain volume (100 mL or 50 mL) of the 10 vol% methanol aqueous solution was mixed with Au-TiO_2 catalyst by ultrasonication for 10 min, forming a homogeneous reaction solution with catalyst concentration of 0.1, 0.3, 0.5, 0.75, 1.0 g L^{-1}. Then the reactor was connected to the pipeline (CEL-SPH2N-D, CEAULIGHT, **Figure S11B**) to extract all dissolved gas in it. After the evacuation, N_2 was injected until the absolute pressure is 0.8 atm in the pipeline and reactor. Then the Xenon lamp was turned on wit convex lens for a 9 h continuous experiment. During the experiment, moderate stirring was maintained during the reaction to prevent aggregation. Two water cooling coils at 0 °C were attached to the photo-thermal reactor to condense any evaporated methanol into liquid, which then flew back to the reactor. The pipeline was equipped with circulation and can collect and mix the gaseous product generated during the reaction. Every 30 min, the gaseous product in the pipeline was auto syringed into the GC7920-TFZA gas chromatography to measure the accumulated hydrogen production. The average hydrogen production rate is calculated when the accumulated hydrogen production becomes linear to reaction time.

Figure S11C shows the hybrid system in operation. The inlet concentrated sunlight is partly absorbed by the photo-thermal reaction solution. The upper quartz window is fixed with an electric heating ring (red colored) as a defogger and heated to 115 °C in operation. This prevents the quartz window from being blurred by the steam of water and methanol reactant. The sunlight unabsorbed by Au-TiO_2 (reddish color) is transmitted downward and leaves the reactor bottom for the bottom PV cell.

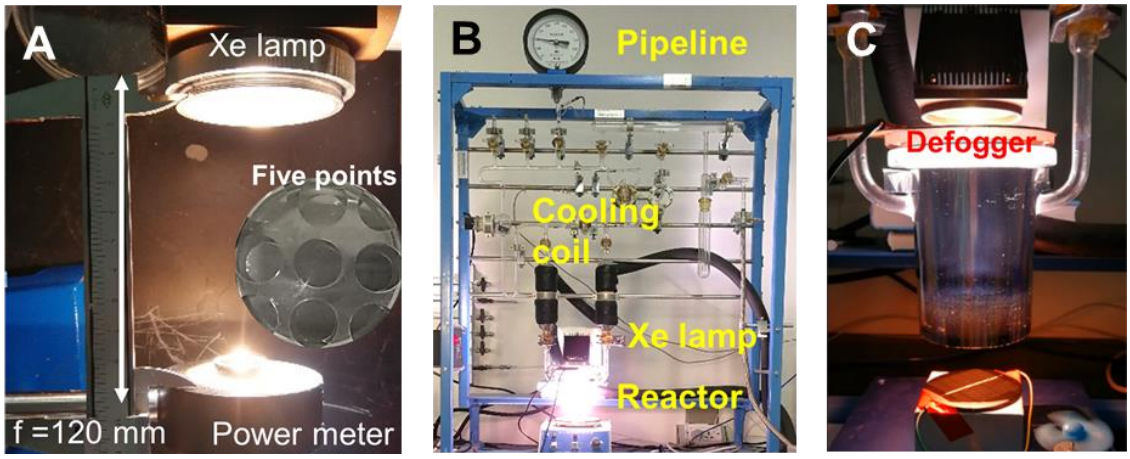

Figure S11. The typical experiment procedure, related to **Figure 2**. (A) Measurement of the average sunlight intensity. (B) Experimental apparatus for the hybrid system under concentrated sunlight. (C) The hybrid system in operation.

Figure S12 shows the preparation of Au-TiO_2 using the deposition-precipitation (DP) method (Sakurai et al., 1993). In the DP method, 1 mol% Au was loaded on Aeroxide P25 TiO_2. In a typical procedure, $HAuCl_4 \cdot 3H_2O$ (0.46 mM, 300 mL) was first added to a three-necked flask and then heated to 80 °C in the oil bath. Then, NaOH (0.1 M) was added to the solution and the pH was adjusted to 7.5. Next, 1 g of TiO_2 was added, and the mixture was stirred at 700 rpm for 3 h. The resultant Au-TiO_2 products were separated and collected with centrifugation, followed by washing with deionized water three times to remove extra Cl^-. The obtained lavender paste was dried in a vacuum oven at the ambient temperature for 24 h and ground to powder.

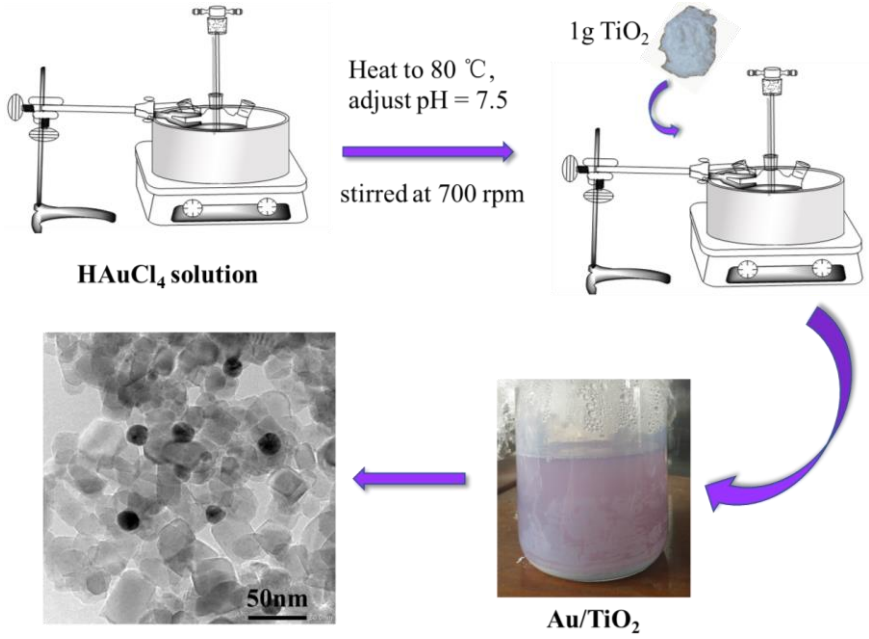

Figure S12. Preparation of Au-TiO_2 photo-thermal catalyst using the deposition-precipitation (DP) method, related to **Figure 2**.

Photocurrent measurement

Figure S13A shows the Au-TiO_2 was fixed on 1 cm × 2 cm indium tin oxide (ITO) coated glass electrodes. The ITO coating has a sheet electrical resistance of 15 Ω/sq. For a typical test, 20 mg of Au-TiO_2 was dispersed homogeneously in 2 mL of 5 wt % Nafion aqueous solution. After 30 mins of ultrasonication, 3-5 drop of the suspension was spin-coated on a piece of ITO glass and put in a vacuum drying oven at ambient temperature for 24 h. To test the stability, the Au-TiO_2 coated electrode was immersed in the electrolyte solution for 24 h and found to remain stable.

Figure S13B-C shows the photocurrent test apparatus. The solar concentration of the Xenon lamp in **Figure S13B** was changed at *C* = 1-9 suns. The sunlight intensity at the electrode position is tested with a CEALL light power meter with measuring range of 0-20 kW m^{-2}. The sensor of the power meter is placed 12.5 cm away from the Xenon lamp, which was the same location of the electrode in photocurrent test. A 2 cm thickness layer of the electrolyte (0.5 M Na_2SO_4 aqueous solution) was placed in front of the power meter sensor as the influence of sunlight attenuation of the electrolyte solution (the inset of **Figure S13B**).

Figure S13C shows the three-electrode system used for the measurement. Considering the neutral PH value of the catalytic solution, the electrolyte was selected as a 0.5 M Na_2SO_4 aqueous solution (Si et al., 2018). The front side of the Au-TiO_2/ITO working electrode was illuminated, and the area of the working electrode dipped in the electrolyte solution was 1 cm^2. The counter electrode was Pt and the reference electrode were Ag/AgCl. All the electrodes were linked to a CHI660e electrochemical workstation. To avoid the influence of the electrolyte temperature, a jacket photoelectrochemical cell with a circulating water bath was used for the measurement. The temperature of the solution was controlled the same as that in photo-thermal hydrogen generation experiments.

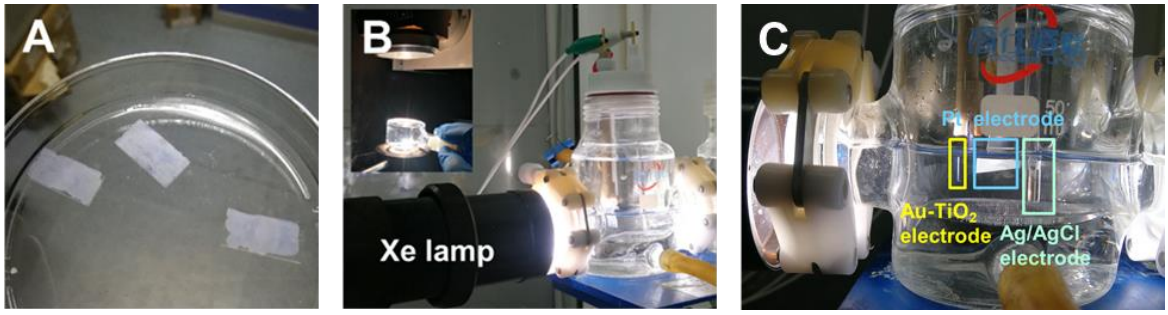

Figure S13. The photocurrent test related to **Figure 4**. (A) The test apparatus. (B) The measurement of simulated sunlight intensity from the Xenon lamp. (C) The three-electrode system.

Voltage-current measurement methods of the PV cell

The voltage-current curve of the PV cell was monitored using a voltammetry measuring method. The measuring mechanism is shown in **Figure S14A**. The voltage-current measurements were made using an DC electronic load (IT8510, ITech), where the inner resistance R_{Adjust} was programmed to sweep the output voltage at 0.2–3.0 V at a sweep rate of 50 mV s^{-1}. The voltage was collected by the inset voltmeter of the DC electronic load (0–18 V, precision: 0.025%+0.025%FS) and the current was collected by an external high precision ammeter (0–500 mA, precision: 0.08%FS). For each set of solar concentration ratio and catalyst concentration, the apparatus scans the voltage from approximately the short-circuit state (0.2 V) to the open-circuit state (3.0 V)

for the voltage-current curve of the PV cell. After the voltage scan, the maximum power point can be found as the maximum of the product of voltage and current.

The experimental setup is shown in **Figure S14B**. The blue reading on the top is from the high precision ammeter, while the green reading on the left at the bottom is from the voltmeter. The readings were collected and depicted into voltage-current curves. In addition to the voltammetry measurement, a 1 W electric fan (blue color) and a 24×0.05 W LED array were used as examples of appliances. The continuous operation of the appliances is shown in **Video S2** and **S3**.

Figure S14C shows the measurement of average sunlight intensity transmitted downward from the reactor bottom. Before each set of PV voltage-current measurement, the transmitted sunlight intensity is measured by the five-point average method same as that used for measuring the average sunlight intensity at the focus. The sunlight intensity at each point is measured by the light power meter with measuring range of 0-20 kW m^{-2}.

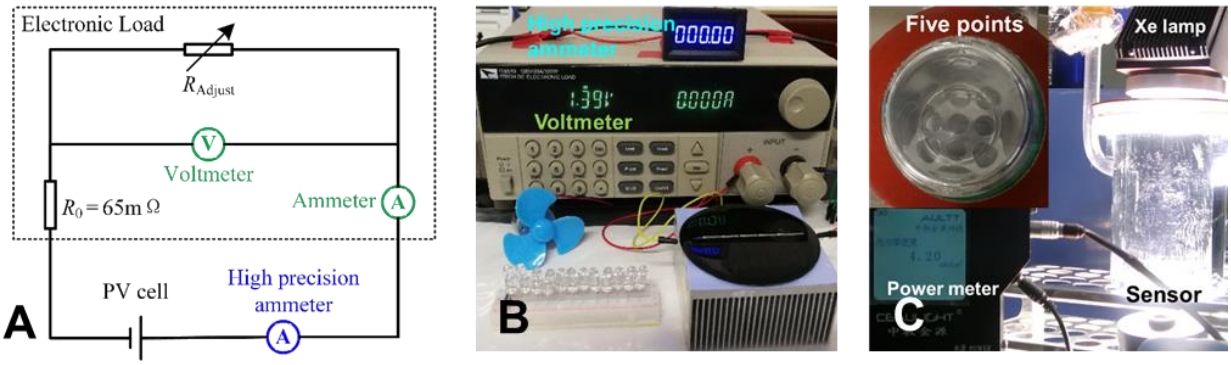

Figure S14. The voltage-current measurement related to **Figure 7.** (A) Measurement circuit. (B) The real setup of the measurement circuit. (C) The measurement of the transmitted sunlight intensity.

Energy flow analysis methods

We analyzed the energy flow at full spectrum to explain the reduction in energy loss through cascading utilization. For the upstream solar concentration and spectrum selecting processes, the energy balance is

$$CI = A(\lambda)\cdot CI + (Q_{trn} + R_{sca}) + (1 - T_{lens}(\lambda))\cdot CI + L_{sca} \quad \text{(S1)}$$

In Eq. S1, the input is the full-spectrum concentrated sunlight *CI* and methanol consumption $\Delta G_{CH4O}\cdot n_{CH4O}$. The amount of the energy in methanol is shown as percentage of the input sunlight. In the spectrum selection process, the photo-thermal reaction system absorbs the narrow-band sunlight $A(\lambda)\cdot CI$ while transmitting the other band Q_{trn} for PV. The optical loss, $(1 - T_{lens}(\lambda))\cdot CI$, occurs at the concentrator lens and the quartz window of the reactor. The scattering occurs on the Au-TiO_2 nanoparticles with some recovered by the reflective film as R_{sca}. All the terms in Eq. S1 can be measured experimentally, and then the scattering loss L_{sca} can be calculated.

For the downstream photo-thermocatalysis and photovoltaic processes, the energy balance is expressed as follows.

$$A(\lambda)\cdot CI + \Delta G_{CH4O}\cdot n_{CH4O} = L_r + L_{heat} + \Delta G_{H2}\cdot V_{H2}/22.4 \quad \text{(S2)}$$

$$R_{\text{sca}} + Q_{\text{trn}} = L_{\text{PV}} + P \quad \text{(S3)}$$

In Eq. S2, the output of the system includes H_2 and PV electricity. Under the absorbed spectrum energy $A(\lambda)\cdot CI$, the photo-thermal reaction generated solar H_2 with chemical energy of $\Delta G_{\text{H2}} \cdot V_{\text{H2}} / 22.4$, plus a recombination loss of L_r. The total input of the PV cell is the sum of the transmitted sunlight Q_{trn} and the recovered scattered sunlight R_{sca}. The corresponding PV electricity output is P, with the energy loss from PV recombination and Ohmic loss as L_{PV}.

Calculation process of individual photo-thermal efficiency

We chose the highest H_2 generation rate at each solar concentration ratio to calculate the efficiency of individual photo-thermal hydrogen production. For example, the 1.0 g L^{-1} has the highest H_2 generation rate among different mass concentrations under C = 12. According to Eq.1, after eliminating the output of PV electricity in the nominator, we have the efficiency for H_2 production

$$\eta_{\text{ptc}} = \frac{\Delta G_{\text{H}_2} \cdot V_{\text{H}_2} / 22.4}{C \cdot \int_{300\text{ nm}}^{2500\text{ nm}} I(\lambda) d\lambda + \Delta G_{\text{CH}_3\text{OH}} \cdot n_{\text{CH}_3\text{OH}}} . \quad \text{(S4)}$$

In the denominator, the Gibbs energy for H_2 is ΔG_{H_2} =237.129 J $mmol^{-1}$ and V_{H_2} is the volume of H_2 (79.9 mL, considered at standard condition) as shown in Figure 5A.

In the nominator, the C is the solar concentration ratio. The incident solar energy is calculated by

$$C \cdot \int_{300\text{ nm}}^{2500\text{ nm}} I(\lambda) d\lambda = C \cdot 3600 \times A \cdot \int_{300\text{ nm}}^{2500\text{ nm}} flux(\lambda) d\lambda$$

Where the A is the irradiated area of a 45 mm diameter round-shape focus. The total solar energy flux $C \cdot \int_{300\text{ nm}}^{2500\text{ nm}} flux(\lambda) d\lambda$ is the solar power flux at the focus. In this case, the $\int_{300\text{ nm}}^{2500\text{ nm}} flux(\lambda) d\lambda$ is 12000 W m^{-2}.

The consumed molar amount of methanol $n_{\text{CH}_3\text{OH}}$ is considered $0.33 n_{\text{H}_2}$ according to the 1:3 stoichiometric ratio to H_2 in methanol reforming, though the consumption of methanol can be much lower in photo-thermal catalysis (Fang et al., 2019). The $\Delta G_{\text{CH}_3\text{OH}}$ here is 726 J $mmol^{-1}$ considering the Gibbs free energy change in methanol combustion reaction.

With all the above, the calculation goes as

$$\eta_{\text{ptc}} = \frac{79.9 \times 237.129 / 22.4}{12000 \times 3600 \times (0.045/2)^2 \times \pi + 726 \times 0.33 \times 79.9 / 22.4} \times 100\% = 1.21\%$$

Supplemental References

Fang, S., Sun, Z. & Hu, Y. H. (2019). Insights into the Thermo-Photo Catalytic Production of Hydrogen from Water on a Low-Cost NiOx-Loaded TiO2 Catalyst. ACS Catal. 9, 5047-5056.

Sakurai, H., Tsubota, S. & Haruta, M. (1993). Hydrogenation of CO2 over Gold Supported on Metal Oxides. Appl. Catal. A Gen. 102, 125-136.

Si, Y., Cao, S., Wu, Z., Ji, Y., Mi, Y., Wu, X., Liu, X. & Piao, L. (2018). What is the predominant electron transfer process for Au NRs/TiO2 nanodumbbell heterostructure under sunlight irradiation? Appl. Catal. B: Environ. 220, 471-476.

Vincenzi, D., Busato, A., Stefancich, M. & Martinelli, G. (2010). Concentrating PV system based on spectral separation of solar radiation. Physica Status Solidi 206, 4.